DOI: 10.1002/anie.200((will be filled in by the editorial staff))

Spherical Multi-Walled Carbon-Nanotube Architectures: Formation Mechanism and Catalytic Performance

Jian Zhang, Rui Wang, Enze Liu, Xufeng Gao, Zhenhua Sun, Feng-Shou Xiao, Frank Girgsdies, Dang Sheng Su**

The chemical-vapor-deposition (CVD) process is sufficiently well developed to allow the large-scale production of carbon nanotubes (CNTs).[1] Metal nanoparticles (Fe, Co, Ni, etc.) are usually immobilized on a solid support and then decompose the gaseous hydrocarbon feedstocks into fragmented carbon units at elevated temperatures of 700-1100°C. Metal carbides are formed and then these dominate the growth of filamentous carbon as a structural template.[2,3] The produced CNTs cannot stay firmly with an inert support and so inevitably detach away, especially during liquid-phase purification or mechanical treatment.[4] The biggest difficulties when handling the loose powder are filtration in the slurry-phase operations and the large pressure drops in fixed-bed reactors. These problems very much limit the application of CNTs on a large scale. The fabrication of carbon filaments on a structured support (e.g., activated carbon, carbon fibers, porous frameworks, graphite)[5,6] has also suffered from discontinuities in the structure. The future use of CNTs has also been restricted by the technical requirements and the necessary high energy consumption to operate the intense and complicated CVD process.

To avoid any mechanical post-treatment of powder and the risk of explosion during CVD synthesis, we have explored a simple method to produce monolithic CNTs directly as millimeter-scale spheres, featuring an integral continuity in the structure from microscopic to macroscopic scales. The whole process of CNTs growth has been conducted in a flow of ultrapure N_2, involving a set of elementary steps in the solid phase being less complex than the widely used CVD process. The growth of CNTs is based on a solid reaction mechanism and well-graphitized nanotubes can be obtained even at a temperature as low as 400°C. Direct observation of all growth events is made by using in-situ transmission electron microscopy (TEM), X-ray diffraction (XRD), IR, Raman spectroscopy and thermogravimetric analysis.

A commercial styrene-divinylbenzene copolymer resin was used as the carbon precursor. According to Scheme 1, the ion-exchanged resin spheres were calcined at 800°C in a flow of N_2 or vacuum, after which the average diameter decreases from 0.77 to 0.49 mm, while the bulk density increases from 0.55 to 0.91 g ml^{-1}. A novel macroscopic structure can be clearly seen, especially after the removal of the Fe nanoparticles and the amorphous carbon species by refluxing the spheres in concentrated HNO_3. As seen in Fig. 1a, the twisted nanotubes construct the monolith while keeping a spherical shape. The cross-section views of the hand-broken spheres show no difference in the structure between the bulk and the surface, indicating a homogeneous distribution of the nanotubes in the millimeter-scale spheres (Fig. 1b). The nitrogen adsorption/desorption isotherm shows a hysteresis loop to identify a typical mesoporous feature. The measured BET surface area and the pore volume are 223.7 m^2 g^{-1} and 0.42 ml g^{-1}, respectively. The distribution of the pores ranges between about 2 and 15 nm.

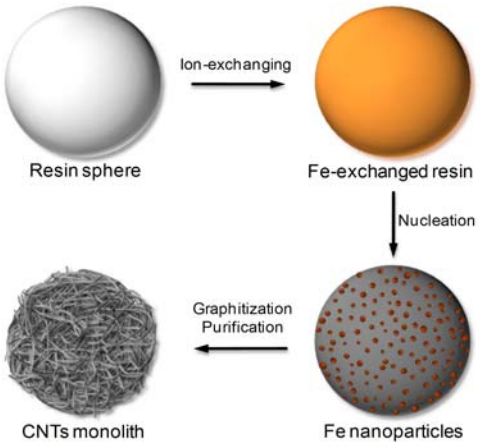

Scheme 1. Schematic figure of the synthesis route to a CNT monolith.

The high-resolution SEM images in Fig. 1a revealed that the produced CNTs are mostly open-end and the inner diameter of the tubes ranges from 60 to 90 nm. Some thin graphitic pieces can be clearly observed as the herringbones on the inner walls (Fig. 1c), but the majority of the tubes were not fully blocked by such dangling graphitic kinks, retaining the open feature of the inner channels. The abundance of microscopic defects inside the channels permits the tight binding of external materials such as metal nanoparticles, proteins, medicine molecules, *etc.* The HRTEM images show the good graphitization extent of the sheath body, ensuring a desirable durability to protect the filling materials. A microforce compressive

[*] Prof. Dr. J. Zhang, Dr. R. Wang, X.F. Gao, Dr. E.Z. Liu, Dr. Z.H. Sun, Prof. Dr. D.S. Su
Shenyang National Laboratory for Materials Science, Institute of Metal Research, Chinese Academy of Sciences
Shenyang, 110016 (China)
Fax: (+86) 24-8397-0019
E-mail: dssu@imr.ac.cn

Dr. Frank Girgsdies, Prof. Dr. D.S. Su
Department of Inorganic Chemistry, Fritz Haber Institute of the Max Planck Society
Berlin, 14195 (Germany)

Prof. F.S. Xiao
Department of Chemistry, Zhejiang University
Hangzhou 310027, China
E-mail: fsxiao@zju.edu.cn

[**] This work is financially supported by MOST (2011CBA00504), NSFC (21133010, 21103203, 50921004, 20973079), Institute of Metal Research (O9NBA111A1), Liaoning Province (20101121), Max Planck Society (Enerchem), and Zhejiang University. We gratefully acknowledge Dr. Di Wang, Jinwei Li, Hao Zhang, Ming Xin, Dr. Bo Zhu and Prof. Feng Li for technical assistances and BESSY for supporting XPS measurements.

Supporting information for this article is available on the WWW under http://www.angewandte.org.

test shows that the spheres can stand a maximum load of 17.6±7.2 N, which is an over 11 times higher crushing force than the nanostructure-free resin spheres that were carbonized under the same conditions, except for using oxalate salts during the ion-exchange treatment. This is helped by the special characteristic of the self-supported nano-architecture of the monolithic CNTs.

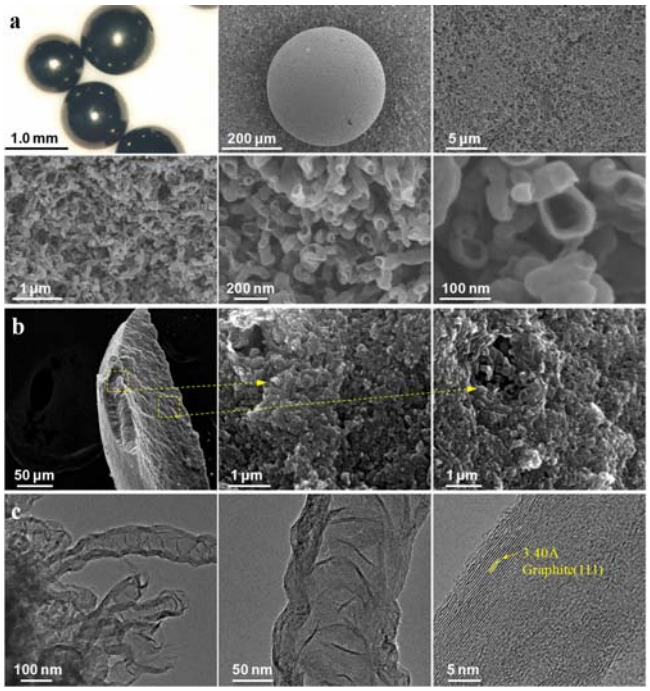

Figure 1. Microscopic images of purified CNT spheres calcined at 800°C. a) Optical microscopy and SEM images at various magnification scales. b) SEM images of crushed sections of purified CNT spheres. c) TEM and HRTEM images of the individual CNTs.

The in-situ microscopic and spectroscopic techniques allowed us to investigate the formation mechanism of the CNTs via a solid-phase route. The in-situ TEM experiments were carried out at specimen temperatures of 400-800°C using heating stages. Figure 2a highlights the sequence of CNT formation at 700°C, when the growth rate is approximately 69 nm min^{-1}. An iron-based nanoparticles fluctuated inside the solid and simultaneously catalyzed the steady growth of one bamboo-like nanotube with an outer diameter of around 37 nm. According to the XRD (data shown later in Fig. 3a) and electron diffraction patterns, the nanoparticles predominantly remain solid or fluctuating crystalline throughout the whole process. The dynamic reshaping of the metal crystals allows them to creep under the barrier of the surrounding carbon solid, leading to the self-supported and porous characteristic of the produced spheres. We were delighted to observe graphitized nanotubes at a temperature as low as 400°C. Figure 2b shows the morphology of a sample that was calcined at 400°C for 4 h. The average outer diameter of the produced nanotubes ranged between 7 and 13 nm. The lattice spacing of 3.43Å reveals the (002) plane of the graphite as being the sheath. The sharp lattice fringes suggest a certain degree of crystallinity, which is very exciting because the solid-phase process can only produce graphitized nanofilaments at above 750°C, according to the available literature.[7]

With the temperature was increased from 650 to 750°C, the estimated growth speed increased from 12 to 305 nm min^{-1}. The Arrhenius plot of the speed against the inverse absolute temperature suggests an activation energy of 254.6 kJ mol^{-1} for this process (Fig. 2c), which is around 30-80 kJ mol^{-1} higher than those of the CVD route.[12] More details can be found in Movies S1 that illustrates one sequence of CNT growth at 700°C. We can clearly see the movements, including nucleation, agglomeration, redistribution and fluctuation, of the Fe-based nanoparticles.

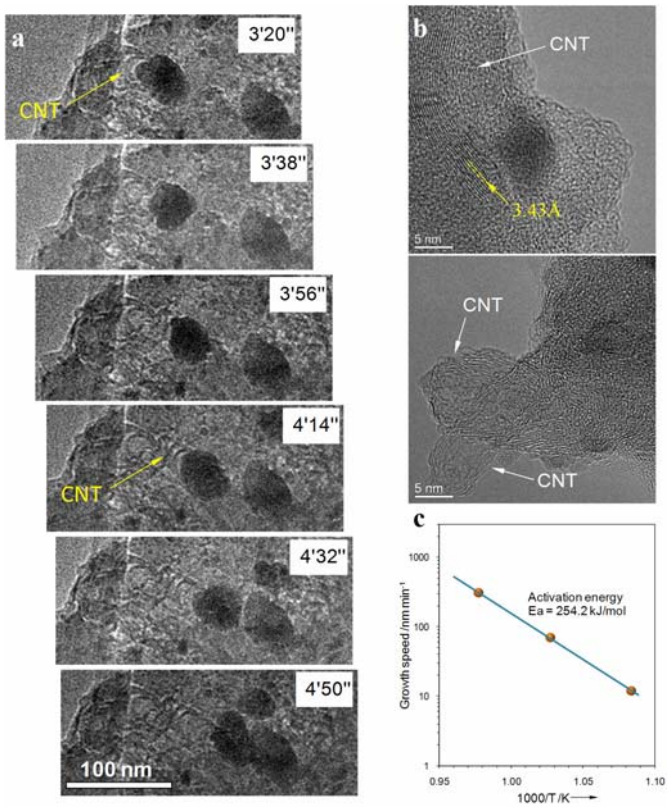

Figure 2. Characterization results of CNT growth via a solid-phase process. a) Time-dependent in-situ TEM images at 700°C. b) Ex-situ high-resolution TEM images of produced iron carbide nanoparticles and carbon nanotubes that were synthesized at 400°C. c) Growth speed of CNTs as a function of inverse absolute temperature.

An in-situ comprehensive characterization using the XRD, DRIFT and Raman spectroscopy made it possible to understand the crystalline state of the nanoparticles as well as the bonding state of the polymeric carbon atoms, which we believe are the key to our synthesis strategy. As shown in Fig. 3a, the transformation of the Fe-based components takes place in three stages, from room temperature to 800°C. A few ferricyanide ions, as the starting precursor, were partially converted into FeO between 200 and 300°C (stage 1), probably assisted by the large quantity of oxygen species, like the hydroxyl groups contained in the resin. The process of thermal treatment was followed by thermogravimetric analyses as part of the temperature-programmed desorption. As seen in Fig. 3b, the weight loss of 21% at 300°C can be primarily assigned to H_2O desorption below 200°C. The peaks of the released CO, CO_2 and H_2O at 240°C and 265°C suggest that the formation of FeO is accompanied by the oxidation of the polymer-type carbon.

A further increase in the temperature transforms the FeO into Fe_3C and Fe_3O_4 (stage 2), during which time the weight of the sample decreased by 11% to release abundant CO, CO_2 and H_2O, peaking at 434-440°C (Fig. 3c). The pronounced diffraction peak of the Fe_3C phase, which is found to catalyze the growth of CNTs during the CVD process in some literature[2,3], therefore makes us believe that the formation of CNTs takes place at a temperature as low as 400°C. The patterns of oxides completely disappear as the temperature reaches 500°C, leaving only metallic Fe and Fe_3C. The

third stage, ranging from 500 to 800°C, mainly involves the phase transformation of Fe_3C, *i.e.,* bainite → cohenite, and metallic Fe, *i.e.,* ferrite (α) → austenite (γ). At 800°C, the crystalline forms only include austenite, cohenite and graphite.

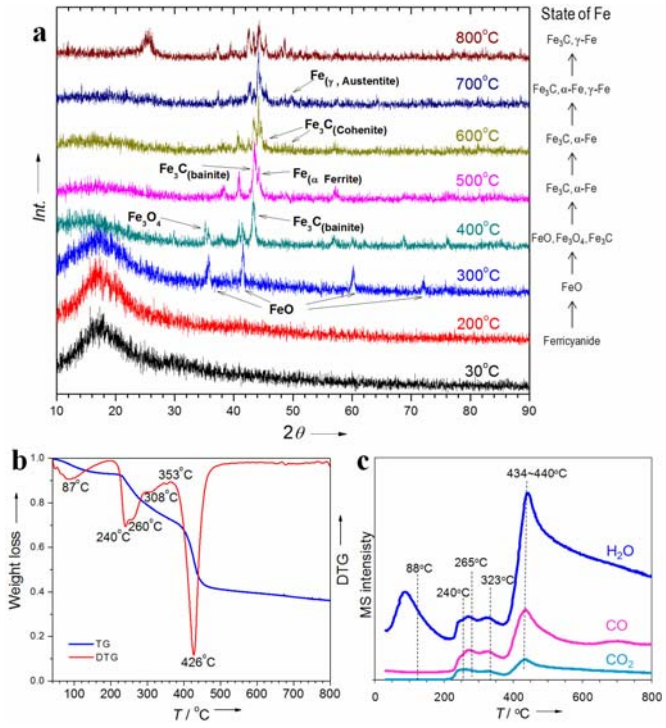

Figure 3. In-situ powder XRD patterns (a) along with the synthesis route up to 800°C. Thermal analysis (b) and mass spectra (c) during TG-DSC experiments with a mass spectrometer to monitor the product mixture in the effluent. Conditions: heating rate 5°C min^{-1}, Ar 40ml min^{-1}.

Fourier-transform infrared spectroscopy helped us to identify the change of the chemical bonding along with the heating procedures. As seen in Fig. 4a, the fresh sample displays all the features of styrene-divinylbenzene copolymer and ferricyanide. The wide band ranging from 3300 to 3600 cm^{-1} reveals the hydroxyl stretching vibrations, while the lower ones at 3020 and 2923 cm^{-1} are attributed to the asymmetric vibrations of the aromatic ring and the aliphatic C-H bonds in the polymer matrix, respectively.[13] As the temperature was increased up to 260°C, a gradual attenuation and the final disappearance of the three important components were observed: ferricyanide as the Fe precursor (2101 and 2030 cm^{-1}), substituted phenyl rings in the polymer matrix (1611, 1511, 1487 and 1458 cm^{-1}), and the aromatic ring C-H bonds in the polymer matrix (1019, 975, 890 and 827 cm^{-1}).[14,15] Based on the appearance of the FeO crystals at 300°C in Fig. 3a, we therefore conclude that, in stage 1, the nucleation of FeO takes place and, simultaneously, the cross-linked polymer framework is destroyed. The latter comprises the scission of C-C and C-H bonds in both the aliphatic and phenyl units with the release of CO, CO_2 and H_2O.

In-situ Raman tests confirmed the disappearance of the aromatic and aliphatic C-H stretching (2900-3100 cm^{-1}), and the benzene skeletal stretching (1583-1613 cm^{-1}) modes[16] at around 270°C (Fig. 4b). The process of carbonization was clearly observed at 380°C, as shown by the *D* and *G* bands at 1340 cm^{-1} and 1583 cm^{-1}, respectively. The *D* band shifted downwards at 1331 cm^{-1} as the temperature reached 400°C, indicating an enhanced domain size of the graphitic structure and a decreased amount of amorphous carbon.[17] This phenomenon can be related to the catalytic growth of the CNT structure in this temperature region (Fig. 2b).

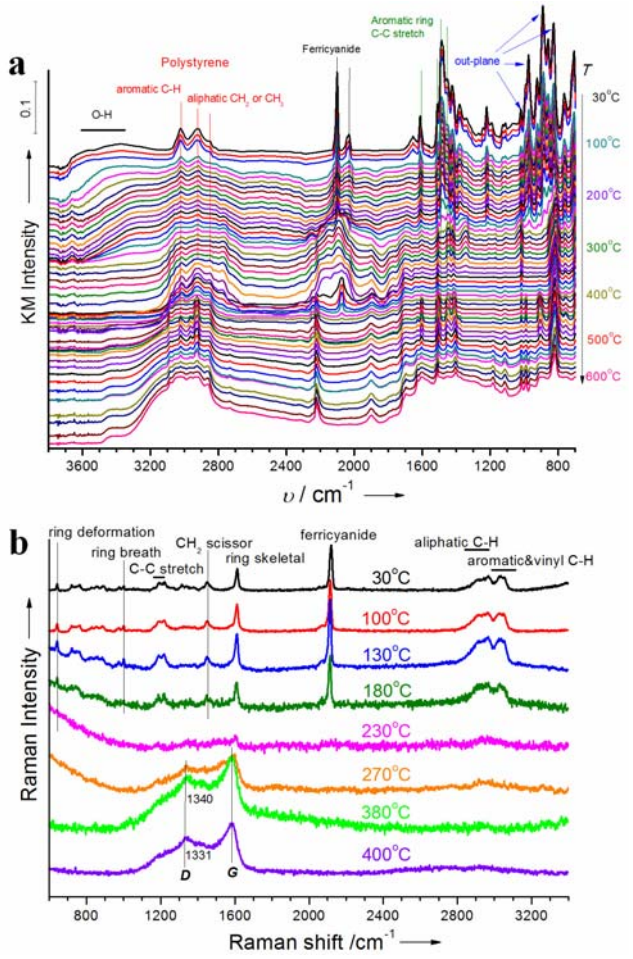

Figure 4. In-situ spectroscopic results of the CNTs growth process from the ferricyanide ions exchanged resin powder that was heated inside the in-situ cells. a) DRIFT patterns ranging from 30 to 600°C. b) Raman patterns ranging from 30 to 400°C.

In our case, the forms of iron are ferricyanide ions, ferrous oxide, iron carbide and metallic iron. The temperature triggers the migration of the ferricyanide ions to destroy their bonding with the polymer matrix. As the temperature reached 260°C, the ionic iron components disappear, while the nucleation into ferrous oxide becomes extremely significant. Ferricyanide ions probably oxidize the surrounding polymeric carbon into CO and CO_2, along with the reduction of Fe(III) to Fe(II) to form the ferrous oxide nanocrystals. Later, at 400°C, the Fe-C interaction becomes more intense and induces the disproportionation of Fe(II) into Fe_3O_4 and Fe_3C, decreasing the sample weight by around 25% to release significant amounts of CO, CO_2 and H_2O. A further increase of the temperature gives rise to the fluctuating carbide nanoparticles and the templating growth of CNTs in large quantities. The extensive diffusion of carbide nanoparticles finally converts the polymer sphere into a porous CNT framework at 800°C.

The surface chemical composition and the functional groups of the purified CNT monoliths were detailed by using synchrotron-excited X-ray photoelectron spectroscopy (XPS). Only carbon and oxygen elements can be identified on the surface of the purified sample (Fig. 5a). Most of the iron elements were removed by refluxing in HNO_3 and the atomic adsorption test only revealed a

weight of Fe equal to 0.2wt%. The residual Fe atoms should be well embedded inside the graphitic framework after we take into account the absence of the Fe signal from the XPS spectra. We were surprised to find that the detected atomic ratio of oxygen was as high as 23.2%, of which the amount of ketonic carbonyl oxygen, peaking at 531.6 eV, reaches 10.1%. We could reasonably expect a satisfactory catalytic activity on a CNT monolith featuring a large amount of active oxygen atoms and an open macroscopic structure.

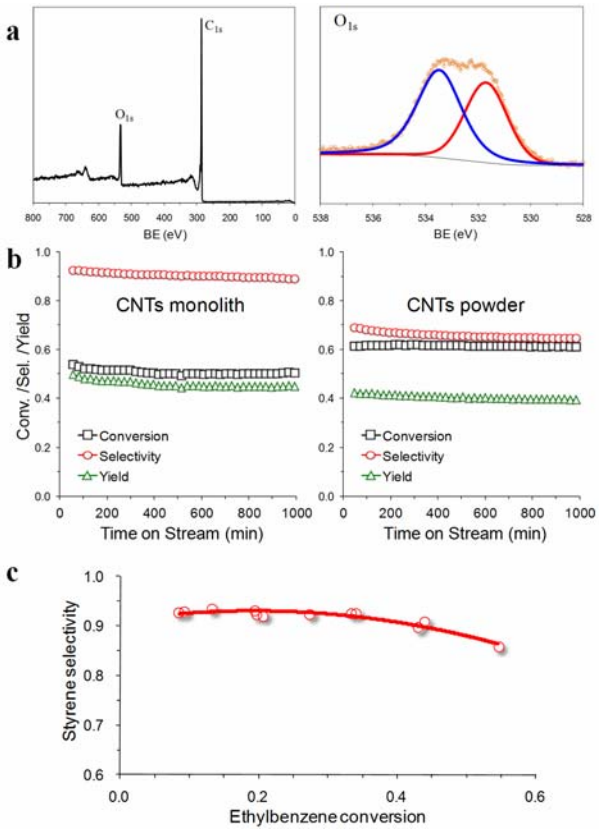

Figure 5. Characterization and catalysis evaluation of purified CNT spheres. a) Survey and O1s XPS spectra of purified CNT monolith. b) Time-on-stream profiles of ethylbenzene conversion, styrene selectivity and yield. c) Conversion-selectivity profiles. Reaction conditions: 100 mg sample, 400°C, 2.9% ethylbenzene, 7.2% O_2, He as balance, total flow rate 10 ml min^{-1}.

Oxygen functional groups are known to terminate the deficient sites in CNTs, like edges and structural defects. Compared with metal catalysts, the controllable surface and structure of CNTs gives them the potential to achieve a superior performance, including high activity, being free of coke and environmentally benign.[18-22] However, the reaction is always performed on a fixed-bed reactor and fine powders with the presence of a hot spot as well as a pressure drop. The use of a bulky, monolithic catalyst that is free of a pressure drop, such as a spherical monolith, is very desirable. The catalytic performance of the CNT monolith spheres was evaluated for the oxidative dehydrogenation of ethylbenzene. Figure 5b shows the outstanding performance of the CNT monolith at 400°C. Its activity is similar to commercial CNT powder, yielding almost the same styrene yield, while the monolith displays a superior selectivity, *i.e.,* around 90%. In comparison, the pure CNT powder only gives a value of 68%. Figure 5c illustrates the conversion-selectivity relationship that is normally used to describe the capability of a single catalysis material. The selectivity of the unsaturated product is known to show an inverse proportional dependence on the conversion of the alkane. For the CNT monolith, the selectivity remains as high as 87%, even at a conversion of 55%. This can be related to the advantage of the monolithic structure in allowing the immediate diffusion of the styrene product.[23] Moreover, the ODH process, as an alternative to direct dehydrogenation (DH), has been limited by its low selectivity and the safety issues relating to the handling of combustive reactants. The CNT monolith is much more selective than the reported ODH catalyst, being close the selectivity of the DH reaction, e.g., 93~97%. Both spherical architecture and tubular nanostructure keep intact after HNO_3 refluxing and oxidative dehydrogenation reaction. Note that the CNT monolith-based ODH process is much more energy-saving than the industrial DH process that is performed at around 630°C with cycling of an excessive amount of steam as the protection agent.

We have shown that the graphitization of an ion-exchanged resin can produce structured CNTs directly via a solid-phase process and presented the detailed changes taking place with the Fe and carbon elements at elevated temperatures. The growth process of the tubular carbon goes through a series of details, including the nucleation of iron oxides, their reaction with the polymer framework, iron carbide formation, the catalytic growth of graphitic tubes and, finally, the production of monolithic CNTs. The solid-phase growth events greatly differ from our present knowledge about the chemical-vapor-deposition processes, providing a more complete understanding of the metal-carbon interaction governing the formation of a carbon nanostructure.[24] This simple methodology, based on widely available chemical feedstocks, should promote the large-scale production of CNTs and the associated applications of CNTs in the near future.

Experimental Section

0.5 g potassium ferricyanide was dissolved in 25 mL ultrapure water to form a transparent solution. 4 g styrene-divinylbenzene copolymer resin spheres were immersed into the solution. The ion-exchanged resin was then washed by ultrapure water to remove the weakly adsorbed ions. After drying overnight, the spheres were put inside a tube furnace for heat treatment. In a flow of ultrapure N_2 (99.995%), the temperature was increased to 400-800°C and held for 4 hours. After the system was cooled down to room temperature, the calcined spheres were taken out from the furnace. The residual Fe can be efficiently removed by refluxing in 160 ml of concentrated HNO_3 solution (65%) at 120°C. The mixture was filtered, fully washed with deionized water, and dried at 80°C under air overnight. The resulting solid was purified CNTs monoliths for subsequent tests.

Textural properties (specific surface area, pore size, etc.) were determined by N_2 physisorption at –196°C on a Micrometrics ASAP 2020 instrument. In-situ TEM was performed inside a Philips CM200 FEG electron microscope operating at 200 kV, equipped with a Gatan Tridiem imaging filter and a sample holder that is resistant up to 1000°C. The sample was dispersed on a Cu grid and heated to a high temperature by increasing stepwise the current through the heating filament. Low-dose electron-beam imaging was used to prevent any beam damage of the sample and any additional heating effect of the electron beam. One image per three seconds was taken using the serial imaging mode and all the images were used to make the video. SEM was made using a Hitachi S4800 electron microscope operating at 3-15 kV, equipped with an EDAX detector. The XPS experiments were carried out at the ISISS beamline in the BESSY synchrotron facility at the end station of the FHI-MPG.

In-situ powder XRD experiments were performed on a STOE diffractometer (Cu Kα radiation, λ = 1.5418 Å) in Bragg-Brentano geometry equipped with a secondary monochromator and a scintillation counter. The sample was heated to the target temperature in a flow of helium, controlled by a mass-flow controller. In-situ diffuse reflectance infrared Fourier-transform (DRIFT) experiments were

conducted on a Thermo Nicolet iS10 infrared spectroscope equipped with a Spectra-Tech Collector II cell and connected with an AVI Omnistar 200 mass spectrometer. In-situ Raman measurements were made using a Thermo Scientific DXR Raman Microscope with a 532-nm laser (50s of exposure time and 50 um slit aperture). All the Ramam spectra were recorded in a N_2 flow (50ml min-1) by heating from room temperature up to 400°C.

Oxidative dehydrogenation of ethylbenzene was carried out at 400°C in a quartz plug-flow reactor with 100 mg of purified CNTs spheres. For comparison, one commercial MWCNTs (Baytube, Bayer Materials) was also treated with concentrated HNO_3 and tested in the ODH reaction under the same conditions. 10 ml min^{-1} of the reactant (1 atm, C_8H_{12}% = 2.9%, O_2% = 7.2%) was then fed to the reactor from a liquid saturator using He as the carrier gas. The reaction products were analyzed with a Varian CP-3800 gas chromatograph equipped with a flame ionization detector for hydrocarbons and a thermal conductivity detector for inorganic components.

Received: ((will be filled in by the editorial staff))
Published online on ((will be filled in by the editorial staff))

Keywords: carbon nanotube · solid synthesis · monolith · oxidative dehydrogenation · catalyst

[1] a) Ç. Öncel, Y.Yürüm, *Fullerenes, Nanotubes, and Carbon Nanostructures* **2006**, 14, 17-37; b) J.-P. Tessonnier, D.S. Su, *ChemSusChem* **2011**, 4, 824-847; c) Q. Zhang, J.-Q. Huang, M.-Q. Zhao, W.-Z. Qian, F. Wei, *ChemSusChem* **2011**, 4, 864-889.

[2] H. Yoshida, S. Takeda, T. Uchiyama, H. Kohno, Y. Homma, *Nano Lett.* **2008**, 8, 208-2086.

[3] R. Sharma, E. Moore, P. Rez, M. M. J. Treacy, *Nano Lett.* **2009**, 9, 689-694.

[4] M. Endo, K. Takeuchi, Y. A. Kim, K. C. Park, T. Ichiki, T. Hayashi, T. Fukuyo, S. Iinou, D. S. Su, M. Terrones, M. S. Dresselhaus, *ChemSusChem* **2008**, 1, 820-822.

[5] D. S. Su, X. Chen, G. Weinberg, A. K.-Hofmann, O. Timpe, S. B. A. Hamid, R. Schlögl, *Angew. Chem. Int. Ed.* **200**5, 44, 5488-5492.

[6] S. S. Tzeng, K. H. Hung, T. H. Ko, *Carbon* **2006**, 44, 859-865.

[7] O. P. Krivoruchko, N. I. Maksimova, V. I. Zaikovskii, A. N. Salanov, *Carbon* **2000**, 38, 1075-1082.

[8] P. J. F. Harris; S. C. Tsang, J. B. Claridge, M. L. H. Green, *J. Chem. Soc., Faraday Trans.* **1994**, 90, 2799-2802.

[9] D. B. Buchholz, S. P. Doherty, R. P.Chang, H. *Carbon* **2003**, 41, 1625-1634.

[10] A. A. Setlur, S. P. Doherty, J. Y. Dai, R. P. H. Chang, *Appl. Phys. Lett.* **2000**, 76, 3008-3010.

[11] R. Sergiienko, E. Shibata, S. Kim, T. Kinota,; Nakamura, T. *Carbon* **2009**, 47, 1056-1065.

[12] M. Pérez-Cabero, E. Romeo, C.Royo, A. Monzón, A. Guerrero-Ruíz, I. Rodríguez-Ramos, *J. Catal.* **2004**, 224, 197-205.

[13] M. Wawrzkiewicz, Z. Hubicki, *J. Hazard. Mater.* **2009**, 164, 502-509.

[14] C. M. Pharr, Griffiths, P. R. *Anal. Chem.* **1997**, 69, 4673-4679.

[15] G. Wronski, S. Pasieczna-Patkowska, Z. Hubicki, *Eur. Phys. J. Special Topics* **2008**,154, 377-380.

[16] E. Partouche, S. Margel, *Carbon* **2008**, 46, 796-805.

[17] J. Schwan, S. Ulrich, V. Batori, H. Ehrhardt, S. R. P. Silva, *J. Appl. Phys.* **1996**, 80, 440-447.

[18] J. Zhang, X. Liu, R. Blume, A. H. Zhang, R. Schlögl; D. S. Su, *Science* **2008**, 322, 73-77.

[19] J. Zhang, X. Wang, Q. Su, L. J. Zhi, A. Thomas, X. L. Feng, D. S. Su, R. Schlögl, K. Müllen, *J. Am. Chem. Soc.* **2009**,131, 11296-11297.

[20] J. Zhang, D. S. Su, A. H. Zhang, D. Wang, R. Schlögl, C. Hébert, *Angew. Chem. Int. Ed.* **2007**, 46, 7319-7323.

[21] J. Zhang, D. S. Su, R. Blume, R. Schlögl, R. Wang, X. G. Yang, A. Gajović, *Angew. Chem. Int. Ed.* **2010**, 49, 8640-8644.

[22] D. S. Su, J. Zhang, B. Frank, A. Thomas, X. C. Wang, J. Paraknowitsch, R. Schlögl, *ChemSusChem* **2010**, 3, 169-180.

[23] J. G. Speight, H. Heinemann, *Structured Catalysts and Reactors*, 2nd Edition, Taylor & Francis Group, LLC., **2006**.

[24] M. Endo, S. Iijima, M. S. Dresselhaus, *Carbon Nanotubes*, Elsevier Science Ltd., **1996**.

Nanocarbon Synthesis

Jian Zhang, Rui Wang, Xufeng Gao, Enze liu, Zhenhua Sun, Fengshou Xiao*, Frank Girgsdie, and Dang Sheng Su* **Page – Page**

Spherical Multi-Walled Carbon-Nanotube Architectures: Formation Mechanism and Catalytic Performance

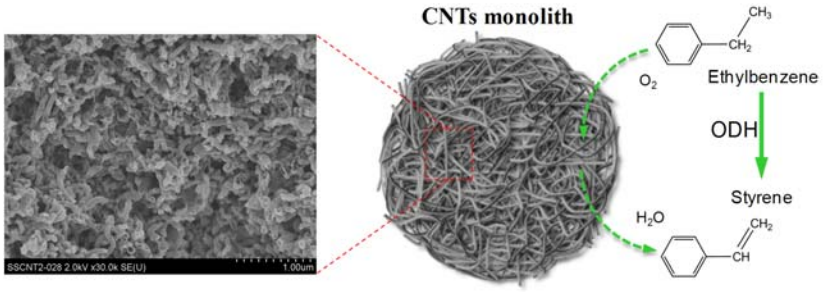

We present a new strategy to produce CNTs sphere via a solid phase process that was well characterized by in situ techniques. The synthesized sphere as a monolith reactor displays an extremely high selectivity in an oxidative dehydrogenation reaction.